Measurement of Pipe and Fluid Properties with a Matrix Array-based Ultrasonic Clamp-on Flow Meter

Massaad, Jack; Van Neer, Paul L.M.J.; Van Willigen, Douwe M.; Sabbadini, Alberico; De Jong, Nicolaas; Pertijs, Michiel A.P.; Verweij, Martin D.

DOI
10.1109/TUFFC.2021.3111710

Publication date
2021

Document Version
Accepted author manuscript

Published in
IEEE Transactions on Ultrasonics, Ferroelectrics, and Frequency Control

Measurement of Pipe and Fluid Properties with a Matrix Array-based Ultrasonic Clamp-on Flow Meter

Jack Massaad, *Graduate Student Member, IEEE,* Paul L. M. J. van Neer, Douwe M. van Willigen, *Graduate Student Member, IEEE,* Alberico Sabbadini, Nicolaas de Jong, *Member, IEEE,* Michiel A. P. Pertijs, *Senior Member, IEEE,* and Martin D. Verweij, *Member, IEEE*

Abstract

Current ultrasonic clamp-on flow meters consist of a pair of single-element transducers which are carefully positioned before use. This positioning process consists of manually finding the distance between the transducer elements, along the pipe axis, for which maximum SNR is achieved. This distance depends on the sound speed, thickness and diameter of the pipe, and on the sound speed of the liquid. However, these parameters are either known with low accuracy or completely unknown during positioning, making it a manual and troublesome process. Furthermore, even when sensor positioning is done properly, uncertainty about the mentioned parameters, and therefore on the path of the acoustic beams, limits the final accuracy of flow measurements. In this research, we address these issues using an ultrasonic clamp-on flow meter consisting of two matrix arrays, which enables the measurement of pipe and liquid parameters by the flow meter itself. Automatic parameter extraction, combined with the beam steering capabilities of transducer arrays, yield a sensor capable of compensating for pipe imperfections. Three parameter extraction procedures are presented. In contrast to similar literature, the procedures proposed here do not require that the medium be submerged nor do they require a priori information about it. First, axial Lamb waves are excited along the pipe wall and recorded with one of the arrays. A dispersion curve-fitting algorithm is used to extract bulk sound speeds and wall thickness of the pipe from the measured dispersion curves. Second, circumferential Lamb waves are excited, measured and corrected for dispersion to extract the pipe diameter. Third, pulse-echo measurements provide the sound speed of the liquid. The effectiveness of the first two procedures has been evaluated using simulated and measured data of stainless steel and aluminum pipes, and the feasibility of the third procedure has been evaluated using simulated data.

Index Terms

Ultrasound flow meter, matrix transducer, parameter extraction, dispersion correction, Lamb waves.

J. Massaad, P. L. M. J. van Neer, A. Sabbadini, N. de Jong, and M. D. Verweij are with the Laboratory of Medical Imaging, Department of Imaging Physics, Faculty of Applied Sciences, Delft University of Technology, 2628CJ Delft, The Netherlands (e-mail: J.M.MassaadMouawad@tudelft.nl).

D. M. van Willigen, and M. A. P. Pertijs are with the Electronic Instrumentation Laboratory, Department of Microelectronics, Faculty of Electrical Engineering, Mathematics and Computer Science, Delft University of Technology, 2628CD Delft, The Netherlands (e-mail: D.M.vanWilligen@tudelft.nl).

P. L. M. J. van Neer is also with the Department of Acoustics and Sonar, TNO, 2597AK, The Hague, The Netherlands (e-mail: paul.vanneer@tno.nl).

N. de Jong and M. D. Verweij are also with the Department of Biomedical Engineering, Thorax Center, Erasmus MC, 3015GD, Rotterdam, The Netherlands (e-mail: M.D.Verweij@tudelft.nl).

Measurement of Pipe and Fluid Properties with a Matrix Array-based Ultrasonic Clamp-on Flow Meter

I. Introduction

ULTRASOUND is widely used to measure flow in industrial environments. There are two major classes of ultrasonic flow meters: in-line and clamp-on. The former typically consists of pairs of single-element transducers positioned inside the pipe and in direct contact with the fluid. The latter generally consists of a single pair of transducers placed on the pipe wall [1]. In both cases, the flow speed will be obtained by measuring the difference between upstream and downstream transit times of the propagating acoustic waves.

The design of in-line flow meters includes a pipe section with known dimensions, around which the transducers are aligned. This alignment depends on the expected range of flow speeds. For very high flow speeds, the acoustic beams might be deflected by the flow, resulting in lower signal-to-noise ratios (SNRs). Nevertheless, since the dimensions of the pipe are known, the acoustic path is completely characterized, and provided the speed of sound of the liquid contents is known, in-line flow meters do not have to be calibrated.

On the other hand, clamp-on flow meters are commonly placed onto pipes whose wall properties (bulk wave sound speeds, diameter, and thickness) and liquid contents properties (sound speed) are not known with enough accuracy or, less often, are completely unknown [2]. Therefore, this type of flow meter needs to be manually calibrated for each pipe. Apart from measuring the pipe and fluid parameters, this calibration consists of manually aligning the transducers by moving these along the pipe and finding the position for which the transmitted acoustic beams are recorded with the highest amplitude (Fig. 1). The main advantage of these flow meters is that, contrary to their in-line counter-parts, they can be installed without interrupting the flow in the pipeline, which represents a valuable advantage in several industries.

The manual alignment procedure of ultrasonic clamp-on flow meters can be tedious when the pipe properties are not known, and also troublesome when working in confined areas. Moreover, pipe imperfections (e.g. corrosion, thickness and diameter variations) remain unnoticed and will not be accounted for when calibrating single-element transducers. Furthermore, even when the axial distance between the transducers in Fig. 1 is found properly, there still remain uncertainties on the pipe properties and geometry, as well as on the sound speed of the liquid. This leads to uncertainties in the conversion of travel time difference into flow speed. Therefore, it would be very valuable to develop a clamp-on flow meter that is able to measure the properties of the pipe and the liquid, find the optimal beam path and proper travel time difference to flow speed translation, and thus automatically calibrate itself prior to metering.

To achieve this, we propose an ultrasonic clamp-on flow meter based on a pair of matrix transducer arrays. With such arrays, we can measure the properties of the pipe (bulk wave sound speeds, diameter, and wall thickness) and the liquid (sound speed). From these parameters, and the beam steering capabilities of matrix arrays, the optimal travel path of the acoustic waves can be automatically found without manual displacement of the sensors.

Information about the material properties and the geometry of solid objects can be extracted from their wave guide modes and/or resonant modes. The use of guided waves has been described in classical texts like [3]–[7], several of which describe the application to pipe walls. Works [8], [9] are a mathematical treatment of acoustic waves scattering from a cylinder or sphere submerged in water. In [9] it is explained that scattering from a submerged sphere is a combination of guided surface modes, and the resonant behavior of its interior. In [10] it is shown that the latter is absent for a fluid filled, submerged cylinder, and that the peaks of the frequency-dependent amplitude of the scattered waves correspond to different guided wave modes of the cylinder wall. In [11], [12], resonances were used to measure the Young's modulus of metallic rods and spheres submerged in water. Ultrasound-Stimulated Vibro-Acoustic Spectrography (USVAS) was used to measure the frequency-dependent amplitude response of the objects, and the resonance that registered a peak amplitude was

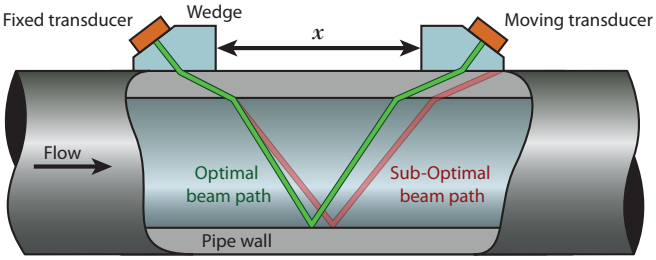

Figure 1: Cross-section of a conventional ultrasonic clamp-on flow meter. The beam path depends on pipe and liquid properties. Before flow metering, the optimal beam path is found by manually moving one of the transducers along the pipe axis, thus varying the separation distance x, until a peak amplitude is measured. For clarity, other beam paths, e.g. those related to helical waves that propagate around the pipe wall, standing waves, shear waves, and the ultrasonic wave reflected by the outer surface of the pipe wall, are not shown.

used to compute the Young's modulus of the objects. However, all these techniques are performed completely underwater without a solid mechanical contact between the transducers and the solid medium. Thus, their implementation is sub-optimal in the setting of ultrasonic clamp-on flow meters.

In this work, we propose to excite and measure dispersion curves of guided waves in the pipe wall using transducer arrays. These curves will depend on the the pipe wall thickness and bulk wave sound speeds. By finding for which combination of parameters the corresponding theoretical curves will best fit the measured ones, these parameters can be extracted. The approach of fitting dispersion curves to extract the elastic parameters of materials has been reported for medical [13]–[15] and industrial [16] applications. However, the fitting process in these cases is performed in a trial-and-error scheme involving the different parameters, and the assessment of the fitting procedure is done more qualitatively (i.e. visual comparison of theoretical dispersion curves with experimental ones) rather than quantitatively. Other approaches [17], [18] are more quantitative with respect to extracting and fitting dispersion curves. However, proper initial guesses of the parameters are needed as inputs for achieving convergence of the optimization algorithms. Furthermore, the approaches have not been tested with ground truth data from simulations, and thus their accuracy has not been verified. In this work, dispersion curves from the measured data are directly compared to pre-computed theoretical dispersion curves for a whole score of bulk wave sound speed and thickness values. Initial guesses of parameters may be used to narrow-down the database search, but they are ultimately unnecessary. Since there is no optimization procedure involved, there are no convergence issues.

Another important parameter to determine in ultrasonic clamp-on flow metering is the sound speed of the liquid. This has been done non-invasively in similar applications. In [19]–[21], transmission measurements were performed with single-element transducers placed in diametrically opposite locations on a liquid-filled pipe to determine the water cut level and the sound speed of different oil-water mixtures. The measured signals contained information from the liquid as well as the pipe wall (i.e. guided waves). The amplitudes associated to the guided waves were estimated based on a priori information about the parameters of the pipe, and subtracted from the measured signal before determining the desired parameters of the fluid. However, in this work, we propose to measure the sound speed of the liquid without needing a priori knowledge of the pipe. A large benefit of using a transducer array, as opposed to single-element transducers, is that a perpendicular pulse echo measurement may be performed to measure the time required for traversing the fluid twice. Moreover, the obtained data may be analyzed in the frequency - horizontal wavenumber ($f - k_x$) domain, where the perpendicular echo related may be singled out by only considering the information centered around the wavenumber $k_x = 0\,\mathrm{rad/m}$.

In this paper, the concept of the proposed measurements, as well as simulation and experimental results are presented. Section II outlines the theory of guided waves. Section III describes the proposed measurement of bulk wave sound speeds and wall thickness of the pipe, along with its implementation on simulated and measured data. Section IV presents a similar outline for the measurement of the pipe diameter. Section V describes the measurement of the sound speed of the liquid on simulated data. In Section VI, the practicalities and limitations of the proposed procedures are discussed. Finally, Section VII highlights the most important conclusions.

II. Guided Waves

The wall of a pipe acts as a waveguide, and when a pipe wall is mechanically excited, dispersive Lamb waves are generated. In a pipe, three types of Lamb wave modes exist: longitudinal, torsional and flexural. The first two modes are axisymmetric, while the last one is not. The mathematical treatment of such waves has been described in [22], [23], and the results are summarized in [7].

Generally, ultrasonic clamp-on flow meters operate in a frequency range from $0.2\,\mathrm{MHz}$ up to $2\,\mathrm{MHz}$ [1]. In many flow metering scenarios, the pipe circumference is much larger than the wavelength of the acoustic waves propagating in the pipe wall, i.e. $\lambda \ll 2\pi R$, with R being the pipe radius. Therefore, the approximation of a flat plate can be made [24], and the dispersion behavior of longitudinal Lamb wave modes in pipes may be described by the Rayleigh-Lamb equation for symmetric modes:

$$\frac{\tan(qh)}{\tan(ph)} = -\frac{4k^2pq}{(q^2-k^2)^2}, \tag{1}$$

and for anti-symmetric modes:

$$\frac{\tan(qh)}{\tan(ph)} = -\frac{(q^2-k^2)^2}{4k^2pq} \tag{2}$$

In Eqs. (1) and (2), k represents the wavenumber, h represents the thickness, and p and q are defined as:

$$p^2 = \left(\frac{\omega^2}{c_L^2}\right)^2 - k^2 \tag{3}$$

$$q^2 = \left(\frac{\omega^2}{c_T^2}\right)^2 - k^2 \tag{4}$$

In Eqs. (3) and (4), ω represents the angular frequency; and c_L and c_T the longitudinal (compressional) and transversal (shear) bulk wave speed in the material, respectively. The solutions to the dispersion equations can be found numerically [7].

Eqs. 1 and 2 assume that the plate has two free surfaces. In the context of ultrasonic clamp-on flow metering, one surface is loaded by a liquid, which modifies the dispersion behavior of the wave modes. However, from Finite Element simulations, it was found that dispersion curves of plates with one water loaded surface deviate from those with two free surfaces only at frequencies below $0.1\,\mathrm{MHz}$, which are outside the operational frequency range of ultrasonic clamp-on flow meters. Therefore, Eqs. 1 and 2 were used as reasonable approximations to develop the methods proposed in this paper.

III. Bulk Wave Sound Speeds and Wall Thickness of the Pipe

The procedure for measurement of the bulk wave sound speeds and the wall thickness of the pipe is based on a quantitative fitting of the measured dispersion curves to the relevant dispersion equations. For simplicity, in this section it will be assumed that the transducer array is directly placed on top of the pipe wall i.e., without a coupling piece.

A. Approach

A cross-section along the axial direction of a clamp-on flow meter with two transducer arrays is shown in Fig. 2. To measure the relevant pipe wall parameters, Lamb waves are generated in the pipe wall by exciting one or several elements of one array, and these are recorded by all the elements of the second array. The measured time-distance ($t-x$) signals can be analyzed in the frequency - horizontal wavenumber (i.e. $f-k_x$) domain, which yields the dispersion curves of the observed symmetric and anti-symmetric modes. The parameters c_L, c_T and h can be found by identifying which combination of these generates the theoretical dispersion curves of (1) and (2) that best match the observed dispersion curves.

In principle, this fitting approach could be implemented for dispersion curves of any order. However, for simplicity, we have worked under the assumption that fitting the A_0 and S_0 wave modes (zero-order anti-symmetric and zero-order symmetric wave modes, respectively) is sufficient to uniquely determine c_L, c_T and h. Below, a description of the curve extraction and fitting procedure is given, followed by its application to numerical and experimental data.

B. Curve Fitting Procedure

To quantitatively compare theoretical dispersion curves to experimental ones, it is first of all necessary to extract the curves from the measured data. In practical terms, converting $t-x$ signals into $f-k_x$ data yields a matrix that associates an amplitude and a phase to each $f-k_x$ coordinate, whereas what is needed is the set of $f-k_x$ coordinates corresponding to a wave mode, i.e. its $f-k_x$ data points. These were identified via the amplitude maxima in the 2D Fourier domain, and their assignment to either wave mode, A_0 or S_0, was performed on the basis of order of appearance along the k_x direction (at every frequency, the horizontal wavenumber k_x belonging to A_0 has a lower value than the one belonging to S_0).

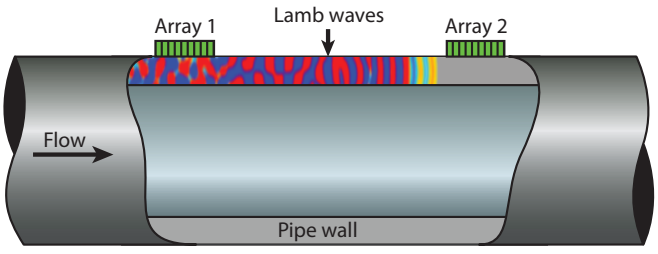

Figure 2: Axial cross-section of a clamp-on flow meter with transducer arrays. For measurement of the bulk wave sound speeds and wall thickness of a pipe, one or few elements of one array can be excited, and the propagating guided waves can then be recorded by the other array.

Next, it is necessary to calculate the theoretical dispersion curves corresponding to different sets of the three parameters c_L, c_T and h, i.e. make a look-up table. Each theoretical curve is then compared to the experimental one, and a measure of error (i.e. the mismatch between the two curves) is defined and computed. Finally, the theoretical curve with the smallest error is identified, thus finding which set of parameters describes the recorded dispersion the best.

An alternative way of approaching this problem would be to implement an optimization procedure to identify the theoretical curve corresponding to the smallest error. The disadvantage of such procedures, however, is that they require the computation of a potentially high number of theoretical curves every time that c_L, c_T and h are sought. With the approach adopted in the present work, the fitting procedure is reduced to comparing every new set of experimental curves to the already existing database. Compared to optimization algorithms, our approach reduces the computational cost considerably since the database can be computed off-line and once (i.e. before the measurements). A potential drawback of this approach is that the accuracy of the fit is limited by the resolution of the parameter space, which is set at the time of the generation of the database. Moreover, similarly to optimization algorithms, there is a trade-off between target precision and computation time: the higher the precision, the larger is the database and the longer the computation time, both for database generation and for the fitting procedure.

The comparison between theoretical and experimental curves was performed by computing the magnitude of an error function that quantifies, at each frequency, the deviation of one curve from the other along the k_x direction. The chosen error function represents the root mean square percentile difference (RMS-PD) between a given theoretical curve and the experimental one:

$$E = \frac{100}{N}\sum_{i=1}^{N}\sqrt{\left(\frac{k_i^{\text{theo}} - k_i^{\text{exp}}}{k_i^{\text{theo}}}\right)^2} \tag{5}$$

In Eq. (5), E is the RMS-PD error, N is the number of frequencies that are considered, k_i^{exp} is the horizontal wavenumber of the i^{th} frequency for the experimental curve, and k_i^{theo} is the horizontal wavenumber of the same frequency for the theoretical curve.

This error function has several advantages: first of all, normalizing the difference at each frequency by the corresponding horizontal wavenumber (either the theoretical or the experimental one) helps to assign the same weight to all points; without this correction, relatively small deviations at higher frequencies impact the error much more than comparable deviations at lower frequencies (a 10% variation from $k_i = 1000\,\text{rad/m}$ is much larger than a 10% from $k_i = 100\,\text{rad/m}$). Moreover, normalizing the error by the number of points used to compute it allows to compare curves where different values of N are used. Finally, a percentile scale is intuitively easy to interpret, even for very small errors.

One last thing that should be noted is that the dispersion curves of the A_0 and S_0 wave modes are not equally sensitive to all three parameters c_L, c_T and h at all frequencies. From theoretical dispersion curves of Lamb waves for a typical set of metallic pipe properties, it was found that the phase speed of the A_0 wave mode, for instance, is sensitive to h mainly at low frequencies (i.e. $f \leq 1\,\mathrm{MHz}$), whereas at higher frequencies it is more sensitive to c_T. The S_0 wave mode, on the other hand, shows a stronger sensitivity to h in the range $1.5\,\mathrm{MHz} \leq f \leq 3\,\mathrm{MHz}$, and is especially sensitive to c_L for $f \leq 1\,\mathrm{MHz}$. This means that any fitting procedure could yield more or less accurate for a given property, depending on which wave mode is fitted at which frequency range.

C. Numerical validation

The procedure described above was first tested on simulated data. A vacuum-loaded stainless steel plate ($c_L = 5800\,\mathrm{m/s}$ and $c_T = 3100\,\mathrm{m/s}$) with a thickness of $h = 1\,\mathrm{mm}$ was simulated using the Finite Element Modelling (FEM) software package PZFlex (Onscale, Redwood City, CA, USA). On one of the surfaces, a small transducer element (HK1HD, TRS Technologies Inc., State College, PA, USA) with a thickness of $0.5\,\mathrm{mm}$ and width of $0.3\,\mathrm{mm}$, was placed and excited with a 1-cycle sine wave with a center frequency of $2.25\,\mathrm{MHz}$. Receivers were placed with a pitch of $0.02\,\mathrm{mm}$ along a distance of $90\,\mathrm{mm}$ next to the excited transducer and on the same side of the plate to record the propagating Lamb waves.

The recorded $t-x$ signals were then transformed into $f-k_x$ data by means of a 2D Fast Fourier Transform (FFT), and the A_0 and S_0 wave modes were then extracted following the procedure explained above (see Fig. 3). The A_0 wave mode was identified within the frequency range $1.5\,\mathrm{MHz} \leq f \leq 2.1\,\mathrm{MHz}$, and the S_0 wave mode was observed within the frequency range $1.5\,\mathrm{MHz} \leq f \leq 2.8\,\mathrm{MHz}$.

Considering the elastic properties of common metals, theoretical dispersion curves were computed for a wide range of fitting parameters: $4500\,\mathrm{m/s} \leq c_L \leq 7500\,\mathrm{m/s}$, $2000\,\mathrm{m/s} \leq c_T \leq 4000\,\mathrm{m/s}$ and $0.1\,\mathrm{mm} \leq h \leq 4\,\mathrm{mm}$, with a sound speed resolution of $50\,\mathrm{m/s}$ and a thickness resolution of $0.1\,\mathrm{mm}$, forming a database of $\approx 10^5$ theoretical curves with a total size of $50\,\mathrm{MB}$. The fitting procedure using this database took $\approx 70\,\mathrm{s}$ on a 64-bit Dell laptop (RAM $= 8\,\mathrm{GB}$, Processor: Intel(R) Core(TM) i7-6600U).

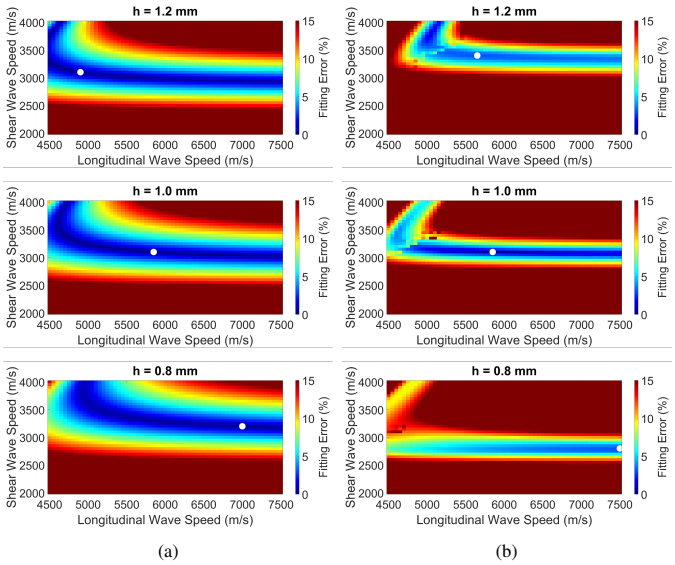

(a) (b)

Figure 4: Error maps obtained by comparing, respectively, the (a) A_0 and (b) S_0 wave mode dispersion curves extracted from simulated data to the theoretical database, for thickness values of $h = 0.8\,\mathrm{mm}$, $h = 1.0\,\mathrm{mm}$ and $h = 1.2\,\mathrm{mm}$. The white dot in each error map indicates the location of minimum error.

Figure 4 shows several 2D error maps, computed via Eq. (5) from the extracted curves and those in the database. These maps show the distribution of the error as a function of the two bulk wave speeds. Each map corresponds to a fixed thickness value h. Fig. 4a and Fig. 4b show the error maps for the A_0 and S_0 wave mode, respectively. From each map, the (c_L, c_T) coordinate that reports the minimum error was extracted. However, to locate this minimum, only those (c_L, c_T) coordinates that report a Poisson ratio relevant for metals, i.e. with a value

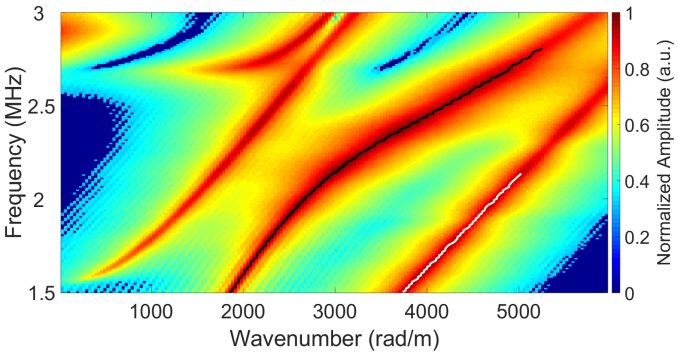

Figure 3: Magnitude of a 2D FFT applied on simulated space-time signals of Lamb waves recorded on the surface of a $1\,\mathrm{mm}$-thick stainless steel plate. The black and white lines show the extracted data points of the S_0 and A_0 wave modes, respectively.

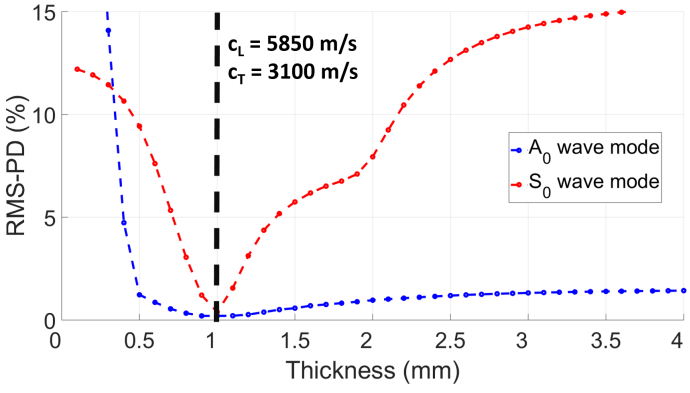

Figure 5: Minimum RMS-PD error of the simulated error maps of Fig. 4, as a function of thickness h, for the A_0 mode (blue) and the S_0 mode (red). The values of longitudinal and shear wave speeds are shown for the thickness $h = 1\,\mathrm{mm}$, which is the one that reports the minimum error.

between $\nu = 0.15 - 0.45$, were considered. Fig. 5 shows, for the two wave modes, a plot of the minimum RMS-PD error as a function of the thickness h. It can be observed that the final parameters obtained via the fitting algorithm were $c_L = 5850\,\mathrm{m/s}$, $c_T = 3100\,\mathrm{m/s}$ and $h = 1\,\mathrm{mm}$. Compared to the simulation parameters ($c_L = 5800\,\mathrm{m/s}$, $c_T = 3100\,\mathrm{m/s}$ and $h = 1\,\mathrm{mm}$), this implies only a discrepancy of $0.86\,\%$ between the values of c_L. Considering that this discrepancy of $50\,\mathrm{m/s}$ is also the speed resolution of the database, it is possible that a database with higher resolution would yield even more accurate results.

D. Measurements

The fitting procedure was applied to measurements obtained from a $40\,\mathrm{mm}$-inner diameter 304-stainless steel pipe (nominal values [25]: $c_L = 5920\,\mathrm{m/s}$ and $c_T = 3141\,\mathrm{m/s}$) with a wall thickness of $h = 1\,\mathrm{mm}$. The sound speeds of Lamb waves in typical industrial pipe walls are much faster than the sound speed of typical liquids. Therefore, these are very likely to be easily windowed-out in time, and for this reason the air-filled pipe setup of Fig. 6a is still representative of a real practical scenario.

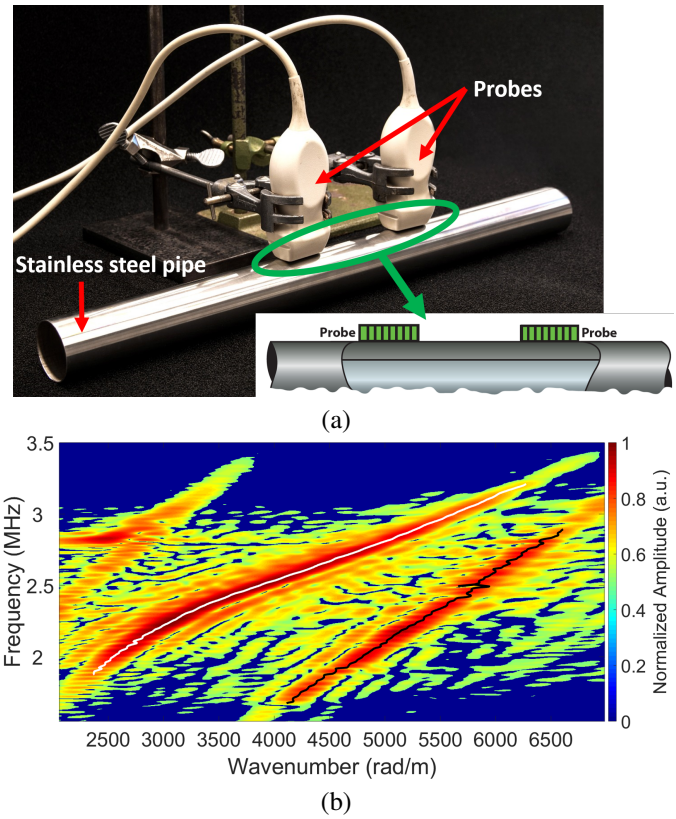

Figure 6: (a) Experimental setup used to excite and measure Lamb waves with transducer arrays on a $h = 1\,\mathrm{mm}$-thick 304-stainless steel pipe (nominal values: $c_L = 5920\,\mathrm{m/s}$ and $c_T = 3141\,\mathrm{m/s}$). The array elements of each probe are oriented along the pipe axis, as indicated by the bottom right schematic. (b) Magnitude of 2D FFT applied on the measured time signals. The black and white lines show the extracted data points of the A_0 and S_0 wave modes, respectively.

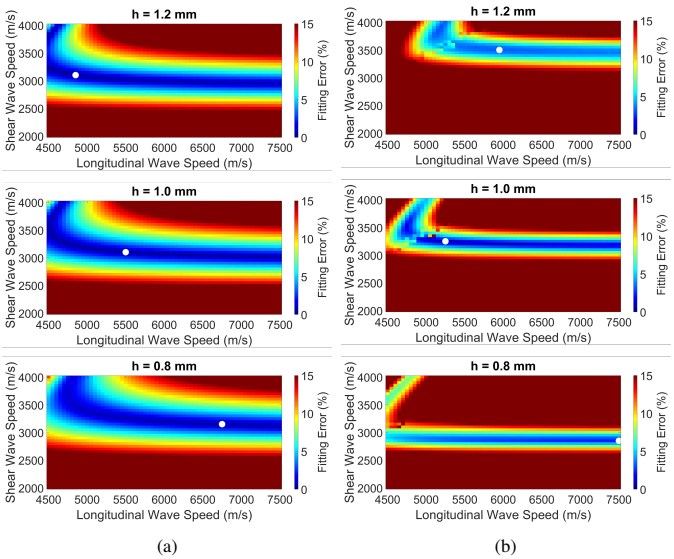

Figure 7: Error maps obtained by comparing, respectively, the (a) A_0 and (b) S_0 wave mode dispersion curves extracted from measured data to the theoretical database, for thickness values of $h = 0.8\,\mathrm{mm}$, $h = 1.0\,\mathrm{mm}$ and $h = 1.2\,\mathrm{mm}$. The white dot in each error map indicates the location of minimum error.

As shown in Fig. 6a, two ATL P4-1 probes (Philips, Bothell, WA, USA) were placed within a center-to-center distance of $10\,\mathrm{cm}$, and driven with a Verasonics Vantage 256 system (Verasonics Inc., Kirkland, WA, USA). A one-cycle square bipolar pulse with a center frequency of $2.25\,\mathrm{MHz}$ was used to electrically excite one element of one probe. The square excitation pulse was translated by the transfer function of the transducer into a sine-like mechanical excitation pulse. All 96 elements of the other probe were used to record the propagating Lamb waves. A 2D FFT was applied on the measured time signals, and from its magnitude (Fig. 6b) the A_0 wave mode was observed within a frequency range of $1.6\,\mathrm{MHz} \leq f \leq 2.8\,\mathrm{MHz}$, whereas the S_0 wave mode was

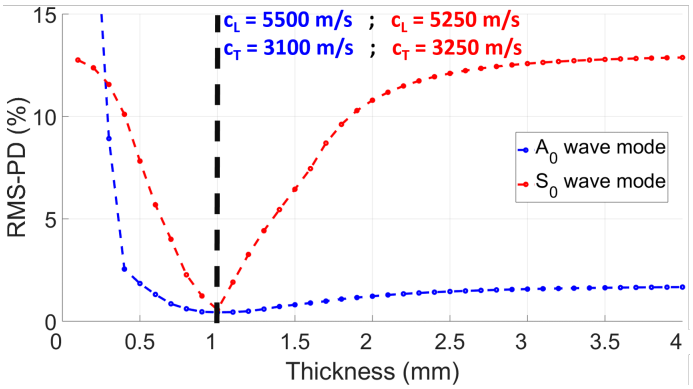

Figure 8: Minimum RMS-PD error of measured error maps of Fig. 7, as a function of thickness h, for the A_0 mode (blue) and the S_0 mode (red). The values of longitudinal and shear wave speeds are shown for the thickness $h = 1\,\mathrm{mm}$, which is the one that reports the minimum error.

identified within $1.8\,\mathrm{MHz} \leq f \leq 3.2\,\mathrm{MHz}$.

Comparing Fig. 3 and Fig. 6b, we notice the effect of noise in the mapping of the dispersion curves obtained from experiments, as well as a difference in spatial resolution of the dispersion curves due to a more limited spatial sampling aperture during experiments. Regardless, the error maps of Fig. 7 and Fig. 8 show that the thickness of the pipe wall is correctly identified when fitting either wave mode. The S_0 wave mode, as already mentioned above and observed from simulations, appears to be more sensitive to thickness variations. Conversely, the values of c_L and c_T extracted by fitting the A_0 wave mode are closer to the nominal properties of the pipe than those found by fitting the S_0 wave mode. The properties reported in Fig. 8 by fitting the A_0 wave mode suggest a discrepancy with nominal values of c_L and c_T of $7.09\,\%$ and $1.27\,\%$, respectively.

The fitting procedure was also applied to measurements obtained from a $62\,\mathrm{mm}$-inner diameter ENAW6063.T66-aluminium pipe (Nedal Aluminium BV, Utrecht, NL; nominal values: $c_L = 6306\,\mathrm{m/s}$, $c_T = 3114\,\mathrm{m/s}$), with a wall thickness of $h = 1\,\mathrm{mm}$. With these measurements it is also shown that the extracted parameters from one dispersion curve may be used as input in the fitting procedure of another curve to obtain more accurate results. For this pipe, $f - k_x$ data points of the A_0 and S_0 wave modes were extracted within the frequency range $1\,\mathrm{MHz} \leq f \leq 2.4\,\mathrm{MHz}$. The properties extracted by fitting each wave mode individually varied considerably from the nominal values. From the A_0 wave mode, values of $c_L = 5100\,\mathrm{m/s}$, $c_T = 3250\,\mathrm{m/s}$, $h = 1.0\,\mathrm{mm}$ were obtained, and for the S_0 wave mode, values of $c_L = 7500\,\mathrm{m/s}$, $c_T = 2950\,\mathrm{m/s}$, $h = 0.9\,\mathrm{mm}$ were obtained. Because at high frequencies the S_0 wave mode is more sensitive to h than the A_0 wave mode, the value of h obtained by fitting the S_0 wave mode was used as input in the fitting procedure of the A_0 wave mode to obtain a more accurate estimate of the bulk wave sound speeds of the pipe. By implementing this approach, values of $c_L = 6700\,\mathrm{m/s}$ and $c_T = 3150\,\mathrm{m/s}$ were finally obtained (see Fig. 9), which represent a discrepancy from nominal values of $8.96\,\%$ and $1.49\,\%$ respectively, with a thickness estimated at $0.9\,\mathrm{mm}$ (a deviation of $10\,\%$ from the nominal value).

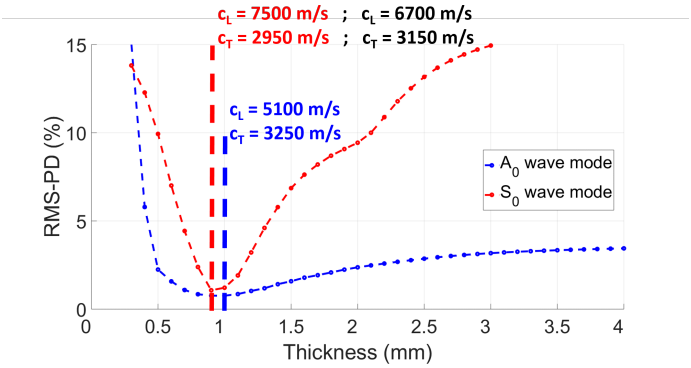

Figure 9: Minimum RMS-PD error of measured error maps for an aluminum pipe as a function of thickness h for the A_0 mode (blue) and the mode S_0 (red). The values of longitudinal and shear wave speeds are expressed for thicknesses with lowest error ($h = 0.9\mathrm{mm}$ for the S_0 wave mode, $h = 1.1\mathrm{mm}$ for the A_0 wave mode). The wave speeds obtained by fitting the A_0 mode with a plate of thickness $h = 0.9\mathrm{mm}$ are reported in black.

IV. Diameter of the Pipe

The average diameter of the pipe is determined by measuring the transit time of a particular Lamb wave traveling around the circumference of the pipe, by looking at the arrival of the envelope of the corresponding pulse. The wave mode is dispersive, therefore, its frequency components will have different transit times $t(\omega)$. Since the dispersive group speed $c_g(\omega)$ of the excited wave mode is known by now, the pipe outer diameter (*OD*) can in principle be computed as:

$$OD(\omega) = \frac{c_g(\omega)t(\omega)}{\pi} + h \tag{6}$$

In practice, however, it becomes challenging to identify the transit time of the measured dispersive signal and the corresponding frequency component. A more accurate estimate of the transit time can be made by performing dispersion correction, i.e. correct for the frequency-dependent phase speed.

A. Lamb Wave Dispersion Correction

Dispersion correction has been applied in non-destructive testing applications at macroscopic [26] and nanoscopic [27] scale. Such correction effectively flattens-out the phase speed dispersion curve of the measured wave mode. After correction, group and phase speed are the same, therefore providing a more accurate estimation of the pipe diameter. Furthermore, since the phase of all frequency components is the same after dispersion correction, a maximum amplitude of the time signal will be achieved at the arrival of the wave, providing the highest possible SNR to estimate the transit time.

Considering a dispersive signal $g(t)$, a frequency component f_0 (associated with phase speed $c(f_0)$) arrives at a time $t(f_0)$. The phase difference between this frequency component and another one is:

$$\Delta\Phi = \omega\Delta t = 2\pi[ft(f) - f_0 t(f_0)] \tag{7}$$

Given that all frequency components travel the same path length p, the following relation holds:

$$p = t(f_0)c(f_0) = t(f)c(f) \tag{8}$$

$c(f)$ represents the phase speed of the measured wave mode. Solving for $t(f)$ in Eq. (8), and substituting the result in Eq. (7), we get:

$$\Delta\Phi = \omega\Delta t = 2\pi t(f_0)\left[\frac{c(f_0)}{c(f)} - \frac{f_0}{f}\right] \tag{9}$$

Given the Fourier Transform of the measured signal $g(f)$, the corrected signal can be computed as:

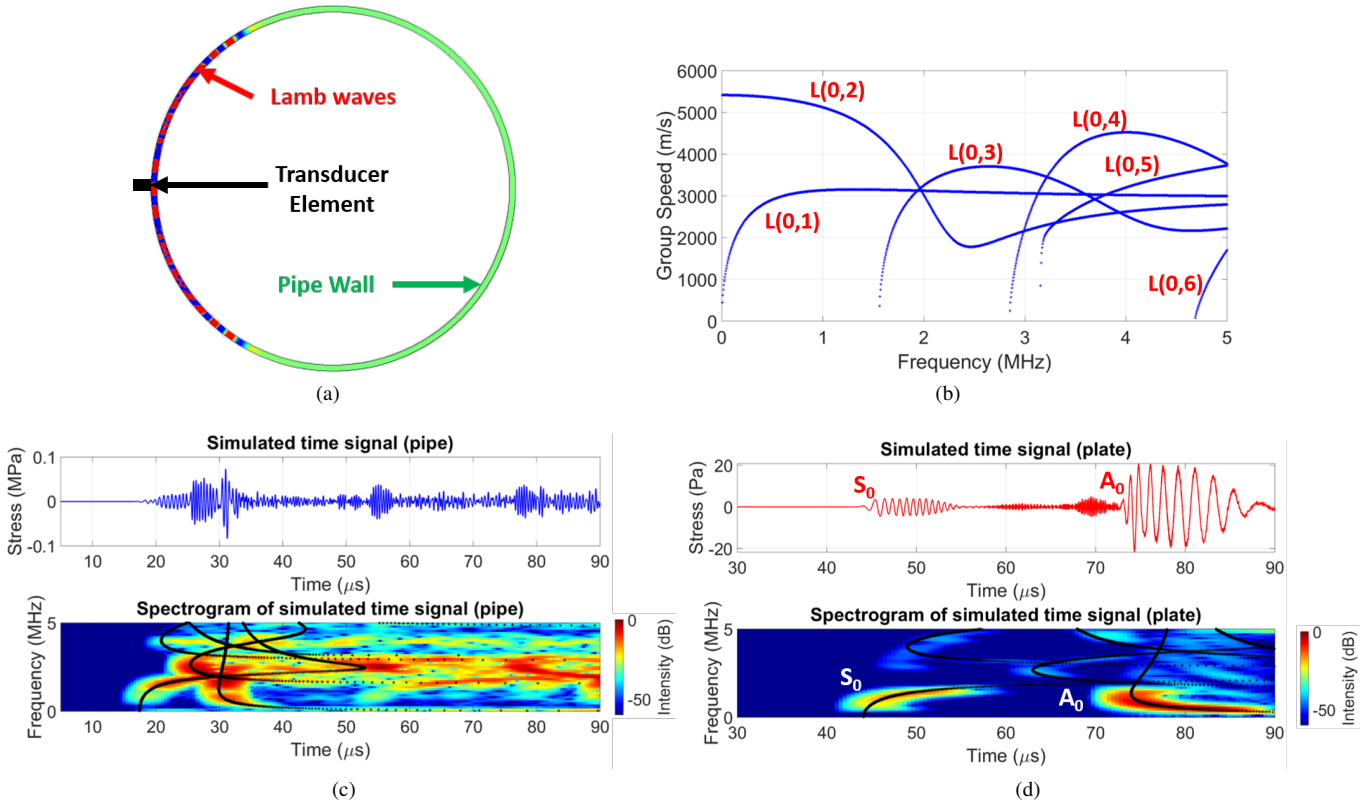

Figure 10: (a) Finite Element simulation of an aluminium pipe ($OD = 60\,\mathrm{mm}$, $h = 1\,\mathrm{mm}$). The transducer element was excited with a 2-cycle sine wave with a center frequency of $2.25\,\mathrm{MHz}$, and receivers were placed around the outer surface of the pipe wall. Transducer element dimensions ($0.5\mathrm{x}0.3\,\mathrm{mm}$) are exaggerated for visualization purposes. (b) Group speed dispersion curves of Lamb waves for the pipe. Around $2.25\,\mathrm{MHz}$, at least three different wave modes are expected to be excited. (c) Simulated stress signal on the opposite side of the pipe and its spectrogram. The black dotted lines are computed from the theoretical group speeds. (d) Simulated stress signal on a flat stainless steel plate, and its spectrogram. The black dotted lines are computed from the group speeds, and overlap with the theoretical curves.

$$g_{\mathrm{corr}}(t) = \mathfrak{F}^{-1}\left\{ g(f) \exp\left[2\pi f t(f_0) \left(\frac{c(f_0)}{c(f)} - \frac{f_0}{f} \right) \right] \right\} \quad (10)$$

where $\mathfrak{F}^{-1}$ represents the inverse Fourier transformation. In Eq. (10) it is observed that only the phase of the signal is being manipulated.

Given a phase speed $c(f_0)$ towards which the dispersion curve is being flattened-out, Eq. (10) is repeated for a given range of transit times $t(f_0)$. For each trial $t(f_0)$, the envelope of the compressed signal is computed and its peak value monitored. The final dispersion-corrected signal would be the one with the highest peak amplitude of its envelope, and the transit time associated to that peak, together with $c(f_0)$, would be the parameters to use in Eq. (6) to finally compute pipe diameter.

B. Simulations

Finite Element simulations of Lamb wave propagation were performed with PZFlex to obtain data that allows us to validate the dispersion correction algorithm explained above, as well as Eq. (6).

The same transducer element as considered in the previous section was simulated on top of an aluminum pipe ($OD = 60\,\mathrm{mm}$, $h = 1\,\mathrm{mm}$), as seen in Fig. 10a. The element was excited with a 2-cycle sine wave with a center frequency of $2.25\,\mathrm{MHz}$. According to the dispersion curves for the pipe, see Fig. 10b, the $\mathrm{L}(0,1)$, $\mathrm{L}(0,2)$ and $\mathrm{L}(0,3)$ wave modes are expected to be excited. Lamb waves were recorded by receivers placed around the outer surface of the pipe wall. From the recorded time signals, a spectrogram was computed considering a moving Hanning window with a time length of $9.5\,\mu\mathrm{s}$. The different wave modes could be identified in Fig. 10c.

To assess the accuracy of the proposed method, a simple flat plate geometry was considered as a valid approximation of a cylindrical pipe wall [24]. Lamb waves were computed $23\,\mathrm{cm}$ away from the source. In the process of validating Eq. (10), the S_0 wave mode in Fig. 10d was considered. After the implementation of the dispersion correction (Fig. 11), the computed travel path was $22.82\,\mathrm{cm}$, which represents a discrepancy of $0.8\,\%$ relative to the true value.

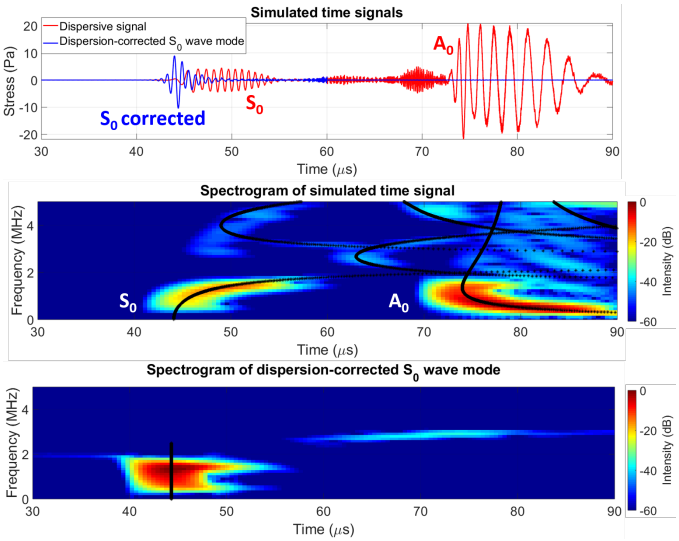

Figure 11: Dispersion correction of the S_0 wave mode computed in a Finite Element simulation involving a stainless steel plate with a thickness $h = 1\,\mathrm{mm}$. The black curves in the spectrograms follow from the theoretical group speeds.

C. Measurements

The proposed procedure for measurement of the pipe diameter was tested on the aluminium pipe described previously. For this purpose, a single ATL P4-1 phase array probe was placed onto the pipe wall in the circumferential direction (Fig. 12). Even though most of the piezo-elements were not in mechanical contact with the pipe wall, the one in the middle of the probe was. This element was then excited with a 2-cycle square pulse with a center frequency of $2.25\,\mathrm{MHz}$. The time

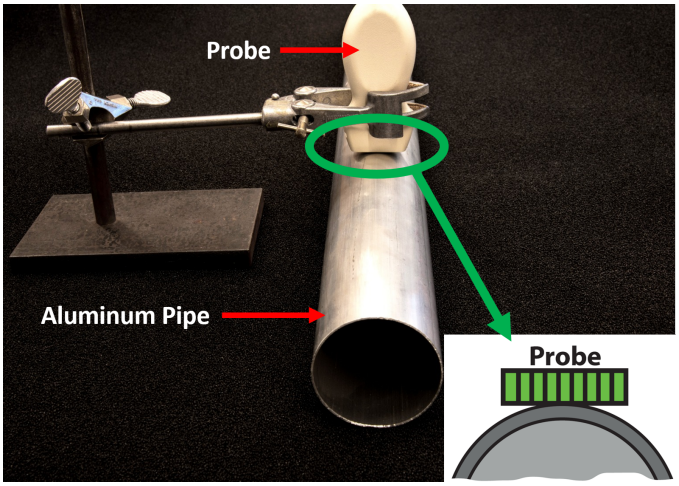

Figure 12: Experimental setup to test the proposed procedure for measurement of the pipe diameter, consisting of an aluminum pipe ($OD = 60\,\mathrm{mm}$, $h = 1\,\mathrm{mm}$), and a P4-1 phased array probe placed on top. The array elements of the probe are oriented perpendicularly to the pipe axis, as indicated by the bottom right schematic. A foam layer was placed below the pipe to avoid mechanical coupling and vibrations of the table on which the setup was placed.

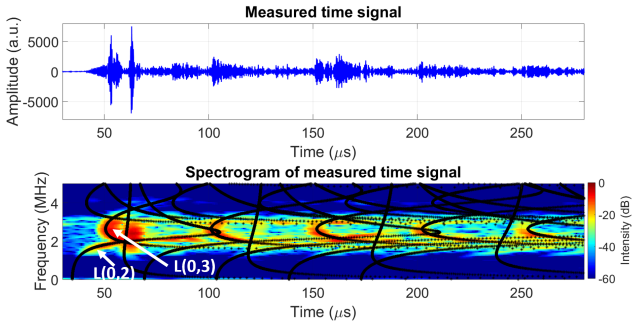

Figure 13: Time signal (above) recorded by one piezo-element of the probe in contact with the aluminum pipe, as shown in Fig. 12, and its spectrogram (below). The black curves in the spectrogram follow from the theoretical group speed computed for the pipe parameters measured in the previous section.

signal recorded by this element, as well as its spectrogram, are shown in Fig. 13, in which several round trips of wave modes, such as the $\mathrm{L}(0,3)$, are observed. Based on the pipe parameters measured in the previous section, group speed dispersion curves were computed and theoretical curves for the maxima in the spectrogram were derived and plotted in the spectrogram. These curves show a very good agreement with the locations of the maxima in the measured spectrogram.

Furthermore, the spectrogram of Fig. 13 shows that the first wave mode to arrive after propagating a full circumference is the $\mathrm{L}(0,2)$. Therefore, this wave mode was windowed-out from the measured time signal and corrected for dispersion. The reference frequency at which the phase speed dispersion curve of this wave mode was flattened-out was $f_0 = 2\,\mathrm{MHz}$. The proposed dispersion correction algorithm was applied with a sound speed of $c(f_0) = 4294\,\mathrm{m/s}$, and the spectrograms of the measured $\mathrm{L}(0,2)$ wave mode before and after dispersion correction are shown in Fig. 14.

After correction, a transit time of $45.4\,\mu\mathrm{s}$ was obtained. When used in Eq. (5), this gives a pipe outer diameter of $OD = 63.05\,\mathrm{mm}$, which implies $5.09\,\%$ discrepancy with the real value. Similarly, measurements were performed for

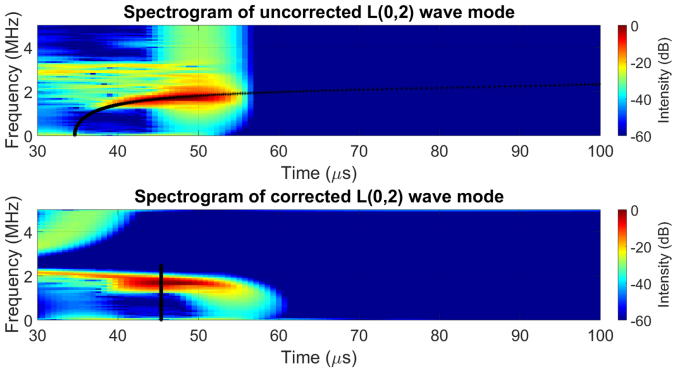

Figure 14: Spectrogram, before and after dispersion correction, of a measured $\mathrm{L}(0,2)$ wave mode on the aluminium pipe shown in Fig. 12. The black curves in the spectrograms follow from the theoretical group speeds.

a stainless steel pipe ($OD = 42\,\text{mm}$, $h = 1\,\text{mm}$), and an outer diameter of $OD = 42.83\,\text{mm}$ was obtained, which means a discrepancy of $1.98\,\%$ with the real value.

Two sources of error were identified. First, it is assumed in Eq. (6) that the piezo-elements are in direct contact with the pipe wall. Since a commercial probe was used to perform the experiments, there is actually a lens between the piezo-elements and the pipe wall, which was not accounted for in Eq. (6). Thus, an effectively longer travel path, and therefore a larger pipe diameter, was obtained. Second, the array probe might have not been placed perfectly perpendicular to the pipe axis. If this was the case, the propagating Lamb wave modes could have travelled around the pipe wall with an angle different from $90°$ relative to the pipe axis, and the travel path of the wave modes might have been longer than the circumference of the pipe. Both errors can be minimized in the future with custom-made transducer arrays designs, such as the one proposed in [28], in which additional path lengths due to the acoustic stack are known and the Lamb waves may be steered to propagate perfectly perpendicular to the pipe axis.

V. Sound Speed of the Liquid

Once the mechanical properties (c_L and c_T) and geometry (h and OD) of the pipe have been characterized, the liquid inside the pipe can also be characterized by measuring its sound speed via pulse-echo measurements. Beam reflections from curved surfaces, such as pipe walls, can modify the waveform and the wave front [7]. To show this effect, a perpendicular cross-section of the measurement setup is considered. Fig. 15 shows the proposed geometry, where a lead coupling piece is placed in between a 16-element transducer array and a liquid-filled stainless steel pipe.

Excitation of all transducer elements produces an initial plane wave that refracts into the pipe. After reflecting from the pipe bottom, the acoustic beam refocuses during propagation in the liquid, refracts back to the coupling piece, and finally impinges the transducer array as a plane wave.

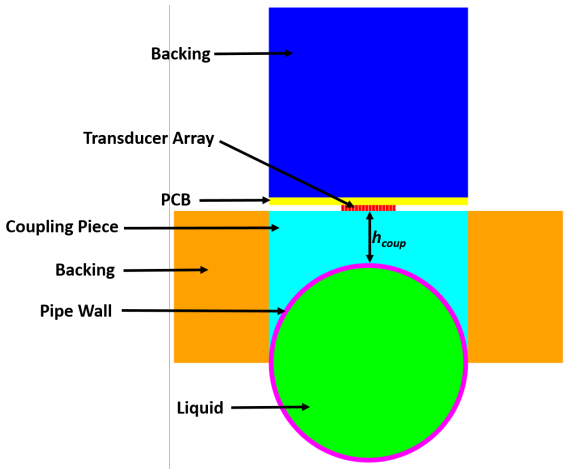

Figure 15: Geometry for measurement of the sound speed of the liquid. A 16-element transducer array is placed on top of a lead coupling piece ($c_L = 2200\,\text{m/s}$, $h_{\text{coup}} = 11\,\text{mm}$) on top of a stainless steel pipe ($OD = 42\,\text{mm}$, $h = 1\,\text{mm}$). The acoustic stack of the array is based on the design described in [28].

Certainly, the recorded time signals would show all possible echoes: those from other interfaces, open ends, and also the Lamb waves traveling around the pipe wall. All these echoes impinge on the array at different angles. Nevertheless, due to the geometry, the echo containing information about the liquid would be the only one impinging completely perpendicular on the array surface. Therefore, in the $f - k_x$ domain, it would show-up as an echo with nearly infinite phase speed (i.e. $k_x \cong 0\,\text{rad/m}$), which could be filtered-out to obtain a cleaner and sharper echo, from which a transit time t_a could be finally determined. From this transit time, the sound speed of the liquid c_{liquid} is computed as:

$$c_{\text{liquid}} = \frac{OD - 2h}{\frac{t_a}{2} - \frac{h}{c_L} - \frac{h_{\text{coup}}}{c_{L_{\text{coup}}}}} \tag{11}$$

where $c_{L_{\text{coup}}}$ represents the longitudinal bulk wave sound speed of the coupling piece, and h_{coup} its center thickness.

Wave propagation in fluids is assumed to be non-dispersive, therefore, no correction needs to be done on the measured echo from the liquid to estimate the transit time t_a.

A. Simulations

A Finite Element simulation of the waves occurring in the geometry shown in Fig. 15 was performed using PZFlex. The set-up involved a water-filled stainless steel pipe ($OD = 42\,\text{mm}$, $h = 1\,\text{mm}$) and a lead coupling piece ($c_L = 2200\,\text{m/s}$, $h_{\text{coup}} = 11\,\text{mm}$). The transducer array elements were excited with a 1-cycle sine wave with a center frequency of $1\,\text{MHz}$, and the received voltage of each transducer element was recorded up to $80\,\mu\text{s}$. To suppress reflections from the open ends of the coupling piece, an attenuating material is placed around it. In simulations, a $20\,\text{mm}$-thick heavy backing (acoustic impedance $Z = 20\,\text{MRayl}$ and attenuation coefficient $\alpha = 20\,\text{dB/MHz.cm}$) was placed around the lead coupling piece. Furthermore, to achieve a real-case scenario, free boundary conditions were implemented at the edges of the simulation geometry. Time snapshots are shown in Fig. 16, where refraction into the pipe wall, as well as refocusing of the acoustic beam after echoing from the bottom of the pipe wall are observed.

The simulated receive voltages from the transducer elements are shown in Fig. 17a, from which it is possible to recognize the characteristic plane wave feature of the water echo, arriving at approximately $63\,\mu\text{s}$. Moreover, it is possible to observe that all the other recorded echoes have a curved shape, which means they arrived at the transducer array under varying angles. The average receive voltage is shown in the blue curve of Fig. 18, and shows a longer duration than the length of the 1-cycle excitation pulse due to the reverberations of the signal in the pipe wall. This means that a cross-correlation operation between these two signals would not be suitable to estimate the transit time of the water echo because the peak value of the cross-correlation, would be located somewhere along the length of the pulse, and not at its actual start. Therefore, a

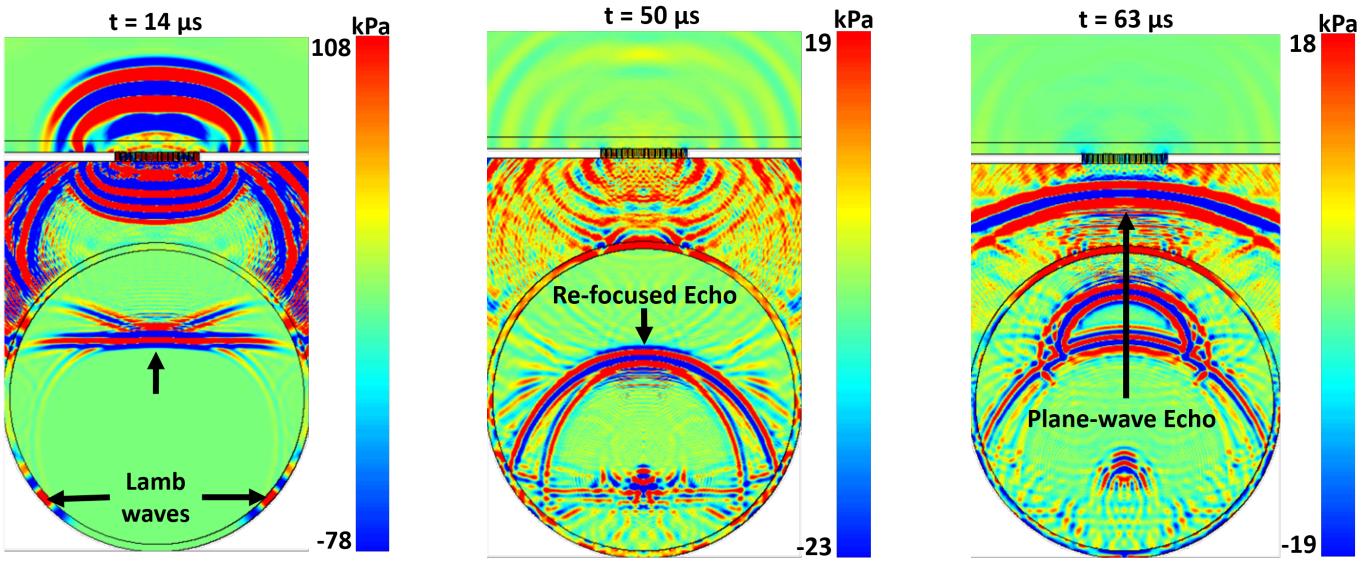

(a) (b) (c)

Figure 16: Snapshots of a Finite Element simulation of the waves occurring in the measurement of the sound speed of the liquid. The simulated set-up contains the array geometry shown in Fig. 15, including a heavy backing material around the coupling piece (not shown here). The pipe was filled with water. (a) At 14 µs, the acoustic wave is propagating downwards. (b) At 50 µs, the wave refocuses after reflecting from the bottom water - steel interface, and propagates upwards. (c) At 63 µs, the wave is about to arrive within the aperture of the array as a plane wave, as expected. The color scale of each snapshot has been clipped to enhance the events indicated with the black arrows.

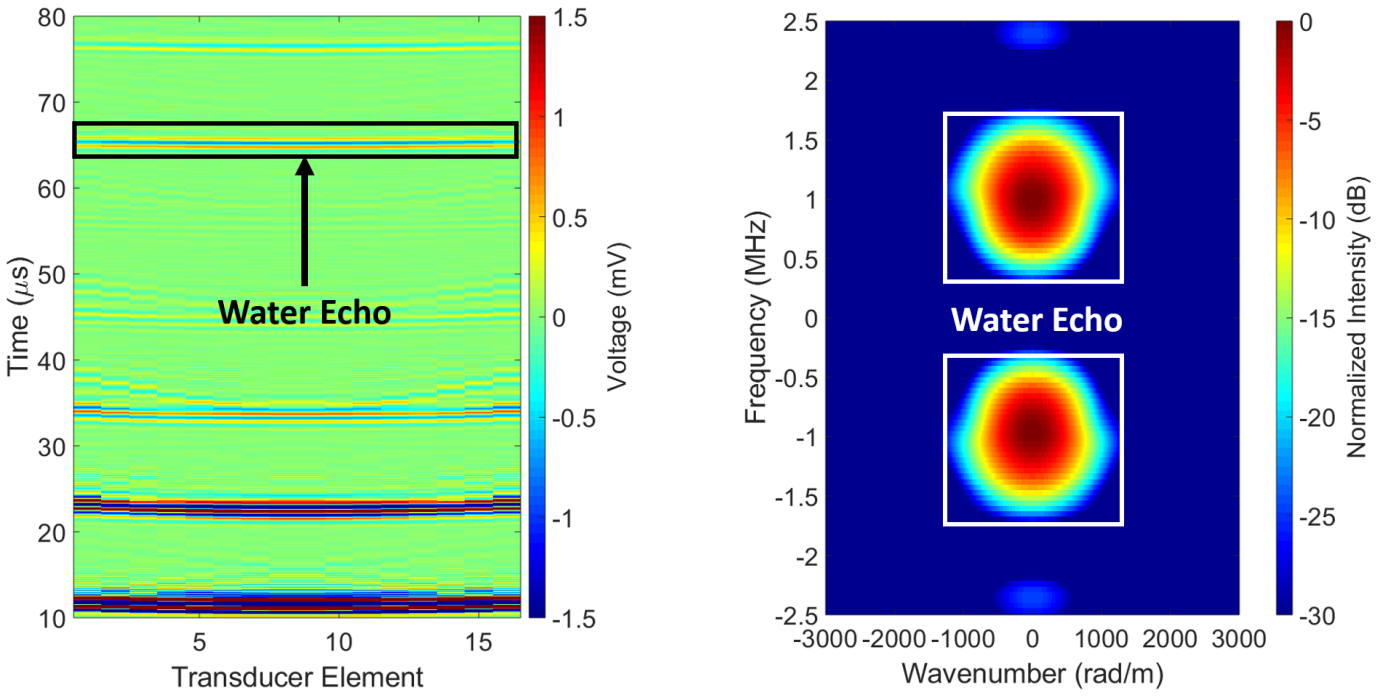

(a) (b)

Figure 17: (a) Simulated receive voltages from the 16-element transducer array shown in Fig. 15. The black rectangle encloses the plane wave water echo. (b) Magnitude of a 2D FFT applied to the tapered data in the time window highlighted in (a). The white rectangles show the band-pass filter applied on the data to dismiss remnant information and achieve a sharper water echo.

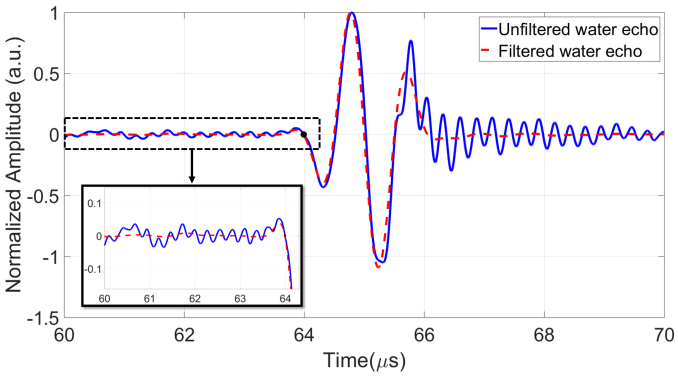

Figure 18: Simulated average and normalized water echo voltages, before and after filtering of the echoes impinging under an angle onto the transducer array surface. After filtering, a smoother echo is observed. The black dot located at $63.99\,\mu\text{s}$ represents the zero-crossing point that marks the transit time of the filtered water echo signal.

zero-crossings tracking algorithm would be more suitable to detect the transit time of the echo from the liquid.

However, detecting the first zero-crossing associated to the start of the acoustic signal may be a bit subjective due to the bandwidth-limited nature of the system, as also suggested by the blue curve in Fig. 18. Moreover, other wave modes may overlap in time with the desired echo from the liquid. Furthermore, Eq. (11) is very sensitive to the transit time being used. Therefore, it would be very useful to apply some filtering to obtain a final signal with a sharper start of the echo and from which to determine the transit time more accurately.

To achieve this, we took the data between $60\,\mu\text{s}$ and $70\,\mu\text{s}$ in Fig 17a, tapered this data in both time and space domain using a Hamming window, and applied a 2D FFT. The result is shown in Fig. 17b, in which the main lobe centered around $k = 0\,\text{rad/m}$ and $f = 1\,\text{MHz}$ corresponds to the plane wave water echo. Within a practical dynamic range of $30\,\text{dB}$, no significant side lobes were present, implying that the implemented tapering is sufficient. By filtering out all the information outside the white rectangles in Fig. 17b and applying an Inverse Fast Fourier Transform (IFFT), filtered time domain signals were obtained. These were ultimately averaged to achieve an echo with a sharper start (see red curved in Fig. 18), from which the transit time can be determined more accurately than the unfiltered version.

An objective method to identify the transit time of the filtered (but still bandwidth-limited) echo may be to scan the time signal from smaller to higher transit times, detect the first amplitude point higher than the noise level, and identify its nearest zero-crossing. The transit time associated to this zero-crossing point may finally be regarded as the transit time of the echo. From the filtered water echo shown in Fig. 18, a transit time of $63.99\,\mu\text{s}$ was obtained, which according to Eq. (11) resulted in a sound speed of the liquid of $c_{\text{liquid}} = 1491.3\,\text{m/s}$. This value has a discrepancy of $0.31\,\%$ with the simulated sound speed value of $1496\,\text{m/s}$ for water.

For measurement of the sound speed of the liquid, it is very important to align the transducer array perfectly perpendicular to the pipe axis. Otherwise, the liquid-related echo might also be recorded under an angle relative to the array surface, and it will be more difficult to differentiate it from all the other echoes. At the moment of writing this paper, the transducer array for ultrasonic clamp-on flow metering proposed in [28] is being fabricated. Furthermore, the use of commercial transducer array probes would make the measurement sub-optimal. Due to the same error source described in Section IV, the acoustic stack inside commercial probes is unknown, which does not allow to account for possible extra path lengths of the acoustic beam inside the probe before reaching the transducer elements. Therefore, is not yet possible to experimentally implement this measurement procedure.

VI. Discussion

The results obtained from simulated data show that the proposed fitting approach is capable of retrieving simultaneously the bulk wave sound speeds (c_L, c_T) and thickness (h) of the pipe wall from a single measurement, without the need for initial guess values. The time required to compare the simulated data to a database of $\approx 10^5$ curves was approximately $70\,\text{s}$, showing great promise for in-situ implementation. Furthermore, the accuracy of this method appeared to be determined by the resolution of the database, implying that the computational cost can be tailored to the accuracy requirements of specific applications. Preliminary results on a steel and an aluminum pipe confirmed experimentally the validity of the approach proposed here. By comparing the retrieved material properties with the nominal values of the samples, it was found that the accuracy of the obtained values was lower in experiments than in simulations, especially for the longitudinal bulk wave sound speed. This discrepancy could be imputed, in part, to experimental limitations (e.g. spatial and temporal resolution) that affect measured data. However, as would appear from Fig. 7, the A_0 and S_0 wave modes are less sensitive to variations of c_L than to variations in c_T and h, potentially impacting the efficacy of the fitting procedure. Moreover, it turned out that the accuracy of the curve-fitting approach increases proportionally to the amount of data points from the wave modes (i.e. $f - k_x$ points) that are available. This means that, to optimize accuracy in practice, it is best to excite the pipe wall with the most broadband signal (i.e. time pulse) possible.

On the other hand, the dispersion effect of Lamb wave modes plays a detrimental role in estimating the outer diameter of the pipe (*OD*), especially if the wave mode is highly dispersive within the operational frequency range of the transducers, which would complicate its isolation from other potential wave modes by e.g. time-windowing. For this reason, two approaches are recommended to estimate *OD*: to excite, within the bandwidth of the transducers, a wave mode with a relatively low dispersive behavior or, if this is not possible, to excite the pipe wall with a relatively narrowband pulse and thereby limit the excitation of many of the highly dispersive frequency components. Another method that might improve the estimation of the pipe diameter would be to cross-correlate consecutive round-trip arrivals of the same

wave mode, like those of the $\mathrm{L}(0,3)$ wave mode shown in Fig. 13. Certainly, each arrival of the wave mode needs to be corrected for dispersion before cross-correlating them. As a consequence of exciting just one transducer array element in the experimental setup of Fig. 12, an acoustic beam with a wide opening angle was generated, which generated all possible Lamb wave modes in the pipe wall and maximized the interference between them, as seen in Fig. 13. Therefore, the measurement setup of Fig. 12 may not always guarantee the possibility to isolate a particular wave mode, as needed by our proposed method. However, in a practical flow meter with matrix transducers, a coupling piece will be placed between the transducer array and the pipe wall, such as the one shown in Fig. 15. In that case, multiple transducer array elements may be used to generate a narrow beam that would impinge the pipe wall under a certain angle, resulting in the generation of only one guided wave mode. Furthermore, with a known dispersion behavior of the guided waves, as determined by the pipe wall thickness and bulk wave sound speeds, wave mode generation could be even more selective by choosing a suitable combination of excitation frequency, pulse length, and beam steering angle.

The matrix arrays can also be used to monitor the quality of their alignment relative to the pipe axis. During sensor alignment, pulse-echo measurements, like those shown in Fig. 17a, can be performed and monitored in real-time. Misalignment of the matrix array(s) would reflect an asymmetric pattern of the $f-k_x$ plots because the echo from the liquid would impinge on the transducer array under an angle relative to the normal of the aperture.

The implementation of our proposed techniques is performed, by a significant amount, in the Fourier domain. This means that the size of the transducer array aperture (given by the pitch times the amount of elements) influences the accuracy of the results by setting a limit on the resolution of the $f-k_x$ representations and spectrograms, and therefore on the ease with which the different dispersion curves are identified and extracted. Moreover, the pitch of the array should be small enough to spatially sample all expected guided waves. The required pitch depends on the involved wavelengths, which in turn depend on the bulk wave sound speeds of the applied metals and the maximum frequency of the employed signals. The $0.3\,\mathrm{mm}$ pitch of the P4-1 probe was enough for proper spatial sampling of the expected wavelengths. Furthermore, the transducer array should remain sufficiently sensitive at lower frequencies , since here the dispersion curves show more sensitivity to the pipe parameters. Based on this point, the $1\,\mathrm{MHz}$ lower cutoff frequency of the P4-1 probe may have not been optimal to achieve the most accurate results. However, the goal of this paper was to prove the feasibility of our proposed techniques. The design of an optimal transducer array for this application is a topic of current research.

VII. Conclusion

In this paper, we have presented procedures for the measurement of parameters that will enable auto-calibration of ultrasonic clamp-on flow meters based on a pair of matrix transducer arrays. With such arrays, pipe properties like wall thickness, bulk wave sound speeds, diameter, and the sound speed of the liquid can be extracted from simulated and measured data. In contrast to a manual calibration approach, the procedures proposed here would reduce calibration time and also produce more repeatable results. Furthermore, these procedures may also be implemented regularly, which in combination with beam steering capabilities of transducer arrays, would allow the flow sensor to be properly calibrated at different pressure/temperature conditions throughout its lifetime. In this way, calibration of ultrasonic clamp-on flow meters by manual displacement of the sensors could be rendered unnecessary.

Acknowledgment

This work is part of the research programme FLOW+, which is financed by the Dutch Technology Foundation STW (project 15031) and industrial partners Bronkhorst and KROHNE.

References

[1] R. C. Baker, *Flow measurement handbook: industrial designs, operating principles, performance, and applications*. Cambridge University Press, 2005.

[2] D. V. Mahadeva, R. C. Baker, and J. Woodhouse, "Further studies of the accuracy of clamp-on transit-time ultrasonic flowmeters for liquids," *IEEE Trans. Instrum. Meas.*, vol. 58, no. 5, pp. 1602–1609, 2009.

[3] I. Viktorov, *Rayleigh and Lamb Waves: Physical Theory and Applications*. Plenum, New York, 1967.

[4] G. Farnell, "Properties of elastic surface waves," *Physical Acoustics*, vol. 6, pp. 109–166, 1970.

[5] P. Chadwick and G. D. Smith, "Foundations of the theory of surface waves in anisotropic elastic materials," in *Advances in Applied Mechanics*. Elsevier, 1977, vol. 17, pp. 303–376.

[6] H. F. Pollard, *Sound waves in solids*. Pion, 1977.

[7] J. L. Rose, *Ultrasonic guided waves in solid media*. Cambridge University Press, 2014.

[8] H. Überall and H. Huang, "Acoustical response of submerged elastic structures obtained through integral transforms," in *Physical Acoustics*. Elsevier, 1976, vol. 12, pp. 217–275.

[9] L. Flax, L. Dragonette, and H. Überall, "Theory of elastic resonance excitation by sound scattering," *The Journal of the Acoustical Society of America*, vol. 63, no. 3, pp. 723–731, 1978.

[10] G. Gaunaurd and A. Akay, "Isolation of the spectrograms and rosettes of insonified sets of submerged, concentric, thin shells," *J. Vib. Acoust.*, vol. 116, no. 4, pp. 573–577, 1994.

[11] M. Fatemi and J. F. Greenleaf, "Application of radiation force in noncontact measurement of the elastic parameters," *Ultrasonic Imaging*, vol. 21, no. 2, pp. 147–154, 1999.

[12] F. G. Mitri, P. Trompette, and J.-Y. Chapelon, "Detection of object resonances by vibro-acoustography and numerical vibrational mode identification," *The Journal of the Acoustical Society of America*, vol. 114, no. 5, pp. 2648–2653, 2003.

[13] K. Heller, L. Jacobs, and J. Qu, "Characterization of adhesive bond properties using Lamb waves," *NDT E INT*, vol. 33, no. 8, pp. 555–563, 2000.

[14] K. Lee and S. W. Yoon, "Feasibility of bone assessment with leaky Lamb waves in bone phantoms and a bovine tibia," *J. Acoust. Soc. Am.*, vol. 115, no. 6, pp. 3210–3217, 2004.

[15] K.-C. T. Nguyen, L. H. Le, T. N. Tran, M. D. Sacchi, and E. H. Lou, "Excitation of ultrasonic Lamb waves using a phased array system with two array probes: Phantom and in vitro bone studies," *Ultrasonics*, vol. 54, no. 5, pp. 1178–1185, 2014.

[16] Y.-C. Lee and S.-W. Cheng, "Measuring Lamb wave dispersion curves of a bi-layered plate and its application on material characterization of coating," *IEEE Trans. Ultrason. Ferroelectr. Freq. Control*, vol. 48, no. 3, pp. 830–837, 2001.

[17] M. Bernal, I. Nenadic, M. W. Urban, and J. F. Greenleaf, "Material property estimation for tubes and arteries using ultrasound radiation force and analysis of propagating modes," *J. Acoust. Soc. Am.*, vol. 129, no. 3, pp. 1344–1354, 2011.

[18] J. Foiret, J.-G. Minonzio, C. Chappard, M. Talmant, and P. Laugier, "Combined estimation of thickness and velocities using ultrasound guided waves: A pioneering study on in vitro cortical bone samples," *IEEE Trans. Ultrason. Ferroelectr. Freq. Control*, vol. 61, no. 9, pp. 1478–1488, 2014.

[19] V. K. Chillara, B. T. Sturtevant, C. Pantea, and D. N. Sinha, "Ultrasonic sensing for noninvasive characterization of oil-water-gas flow in a pipe," in *AIP Conference Proceedings*, vol. 1806, no. 1. AIP Publishing LLC, 2017, p. 090014.

[20] V. K. Chillara, B. Sturtevant, C. Pantea, and D. N. Sinha, "A physics-based signal processing approach for noninvasive ultrasonic characterization of multiphase oil-water-gas flows in a pipe," *IEEE Transactions on Ultrasonics, Ferroelectrics, and Frequency Control*, 2020.

[21] J. Greenhall, C. Hakoda, E. Davis, V. Chillara, and C. Pantea, "Non-invasive acoustic measurements in cylindrical shell containers," *IEEE Transactions on Ultrasonics, Ferroelectrics, and Frequency Control*, 2021.

[22] D. C. Gazis, "Three-dimensional investigation of the propagation of waves in hollow circular cylinders. I. Analytical foundation," *J. Acoust. Soc. Am.*, vol. 31, no. 5, pp. 568–573, 1959.

[23] ——, "Three-dimensional investigation of the propagation of waves in hollow circular cylinders. II. Numerical results," *J. Acoust. Soc. Am.*, vol. 31, no. 5, pp. 573–578, 1959.

[24] A. Velichko and P. D. Wilcox, "Excitation and scattering of guided waves: Relationships between solutions for plates and pipes," *J. Acoust. Soc. Am.*, vol. 125, no. 6, pp. 3623–3631, 2009.

[25] P. Moore, G. Workman, and D. Kishoni, *Nondestructive Testing Handbook, vol. 7: Ultrasonic Testing*, 1991.

[26] R. Sicard, J. Goyette, and D. Zellouf, "A numerical dispersion compensation technique for time recompression of Lamb wave signals," *Ultrasonics*, vol. 40, no. 1-8, pp. 727–732, 2002.

[27] P. L. van Neer, B. Quesson, M. van Es, M. van Riel, K. Hatakeyama, A. Mohtashami, D. Piras, T. Duivenoorde, M. Lans, and H. Sadeghian, "Optimization of acoustic coupling for bottom actuated scattering based subsurface scanning probe microscopy," *Rev. Sci. Instrum.*, vol. 90, no. 7, p. 073705, 2019.

[28] J. Massaad, D. van Willigen, P. van Neer, N. de Jong, M. Pertijs, and M. Verweij, "Acoustic design of a transducer array for ultrasonic clamp-on flow metering," in *IEEE International Ultrasonics Symposium (IUS)*. IEEE, 2019, pp. 1133–1136.